

## Rock-physics modeling for the elastic properties of organic shale at different maturity stages

Luanxiao Zhao<sup>1</sup>, Xuan Qin<sup>2</sup>, De-Hua Han<sup>2</sup>, Jianhua Geng<sup>1</sup>, Zhifang Yang<sup>3</sup>, and Hong Cao<sup>3</sup>

### ABSTRACT

Modeling the elastic properties of organic shale has been of long-standing interest for source rocks and unconventional reservoir characterization. Organic shales exhibit significant variabilities in rock texture and reservoir properties at different maturity stages, subsequently affecting their elastic responses. We have developed a new rock-physics modeling scheme honoring the maturity levels (immature, mature, and overmature), which are constrained by the evolution of the physical properties of organic shale upon kerogen maturation. In particular, at different maturity stages, the manners in which the compliant organic materials interact with the inorganic mineral matrix are characterized by different effective medium theories. On the basis of the developed rock-physics templates, organic shales have different elastic behaviors at different maturity stages. Ignoring the impact of kerogen maturation is insufficient to adequately characterize the elasticity of the whole organic shale system. Modeling results suggest that the elastic responses of organic shale are sensitive to two dominant factors — organic matter content and mineralogical composition. The elastic anisotropy characteristics are not only affected by the kerogen content and clay alignment but also depend on the morphology of kerogen distribution. Our results compare satisfactorily with data from ultrasonic velocity and log measurements, confirming validity and applicability of our modeling framework.

### INTRODUCTION

Given the importance of organic-rich shale as source rocks and unconventional reservoirs, it is imperative that a thorough understanding of shale rock physics is developed. Such rock-physics re-

lations are essential to interpret and predict sonic measurements and seismic responses in terms of identifying sweet spots and characterizing source rocks. The aim of this study is to model the elastic properties of organic shale at different maturity stages, which relates its microstructure and composition to the effective elastic behavior as organic matter thermally matures.

The organic shale is unique in that it contains organic and inorganic components, and this makes organic shale undergo a more complex geologic process. The fine-grained inorganic particles, including rigid grains of quartz and calcite and ductile grains of clay, typically undergo initial sedimentation, dehydration, compaction, and cementation. Meanwhile, organic matters also have gone through accumulation, preservation, and compaction along with the fine-grained inorganic particles. When the environment satisfies the condition of maturation, hydrocarbons can be generated through a series of decomposition reactions (Luo and Vasseur, 1996; Carcione and Gangi, 2000), from which we can conceptually classify the process of maturation into three levels (Tissot et al., 1974; Vernik and Landis, 1996; Vanorio et al., 2008): immature, mature, and overmature. At the immature stage, kerogen with a vitrinite reflectance of [Ro (%)] less than 0.5 corresponds to onset of hydrocarbon generation, which is often termed as “oil shale.” At the mature stage, as temperature increases, kerogen with a vitrinite reflectance of [0.5 < Ro (%) < 1.3] corresponds to the main stage of hydrocarbon generation and primary migration. This stage typically covers the oil window and is often called “shale oil.” At the overmature stage [Ro (%) > 1.3], the generated oil cracks to gas. This stage typically covers the gas window and is often called “shale gas.”

Obviously, the kerogen maturation processes involving physical and chemical changes have systematically altered properties of organic shale. More specifically, the composition, texture, microstructure, pore fluids, and organic matter distribution all experience changes during the course of thermal alternation. Ahmadov (2011), Zargari et al. (2013), Kanitpanyacharoen et al. (2014), Yenugu (2014), and Allan et al. (2014, 2015) make extensive investigations

Manuscript received by the Editor 23 December 2015; revised manuscript received 6 June 2016; published online 3 August 2016.

<sup>1</sup>Tongji University, State Key Laboratory of Marine Geology, Shanghai, China. E-mail: zhaoluanxiao@tongji.edu.cn; jhgeng@tongji.edu.cn.

<sup>2</sup>University of Houston, Department of Earth and Atmospheric Sciences, Houston, Texas, USA. E-mail: qin.xuan1@gmail.com; dhan@uh.edu.

<sup>3</sup>RIPED, CNPC, Shanghai, China. E-mail: maggie@petrochina.com.cn; caoho@petrochina.com.cn.

© 2016 Society of Exploration Geophysicists. All rights reserved.

on the fabric and texture evolutions of organic shale with kerogen maturity. Therefore, it is critical to take into account the kerogen maturation processes for shale rock-physics model because rock properties of organic shale are inherently associated with the maturation process (Zargari et al., 2013; Allan et al., 2014; Yenugu, 2014).

Some authors have applied different methods to predict and analyze the elastic properties of organic shale. Vernik and Landis (1996) propose a conceptual modification of the Backus averaging method (Backus, 1962) to incorporate the effect of lenticular pattern of kerogen network in the shale background. Hornby et al. (1994) develop a theoretical modeling scheme, which is based on a combination of anisotropic differential effective medium (DEM) and self-consistent approximation (SCA) methods, to predict the effective elasticity of shale. Lucier et al. (2011) use the Hashin-Shtrikman lower bounds to calculate the elastic moduli for mixtures of mudrock and organic matter, and they find that in the Haynesville Shale gas reservoir, the effect of gas saturation on the  $V_P$ - $V_S$  relation is more significant than that of the total organic carbon (TOC) effects. By assuming spherical oil/gas phase inclusion in a kerogen matrix, Carcione et al. (2011) and Carcione and Avseth (2015) describe the dependence of velocity on kerogen content using the Backus averaging and the Krief/Gassmann models. Zhu et al. (2012) use the solid substitution model to handle the TOC effect by treating organic matter as inclusion infill material with certain bulk and shear moduli. They find that TOC tends to decrease the P- and S-wave velocities, density, and  $V_P/V_S$  ratios and increase the velocity anisotropies. Guo et al. (2013) describe the Barnett Shale brittleness index with isotropic SCA and the Backus averaging method through considering the degree of the preferred orientation of clay and kerogen particles. Vasine et al. (2013) model the elastic

anisotropies of Kimmeridge Shale based on the quantification of microstructural features, such as phase volume fractions, grain shapes and grain orientations, and pore distributions with scanning electron microscope (SEM), transmission electron microscopy (TEM), and X-ray diffraction (XRD) techniques. However, little work has investigated the effect of maturation evolution for modeling organic shale in detail, especially highlighting the distinction of elastic responses at different maturity levels. As a consequence, the correlation between kerogen maturation and the elastic behaviors of shale via rock-physics modeling remains poorly characterized, which in turn makes the seismic responses poorly understood.

This paper presents a framework for modeling elastic properties of organic shale on the basis of its maturity levels, thereby providing insights into the seismic characterization of shale reservoirs. Emphasis will be placed on how the maturation process controls the physical properties of organic-rich shale, and thereby constrains the modeling framework. We propose a modeling strategy using different effective medium theories to simulate the elastic responses of organic-rich shale at immature, mature, and overmature stages, respectively. The modeling framework offers a simple and basic description that can be locally calibrated, although we recognize the difficulty in prescribing a universal set of parameters due to the tremendous variabilities of organic shales worldwide.

The paper is organized as follows: First, a qualitative characterization of kerogen maturation will be presented. In particular, how the interactions between organic and inorganic components vary upon maturation will be illustrated in detail. Then, the modeling framework and detailed modeling steps will be introduced. Following this section, the rock-physics templates (RPTs) for immature, mature, and overmature shales will be explored, respectively. We next apply the modeling methods to the ultrasonic and log data to analyze geologic factors affecting elastic responses of organic shale. Finally, we end with discussions and conclusions.

## ORGANIC MATTER MATURATION CHARACTERIZATION

When organic matter is contemporaneously deposited with geologic material, subsequent sedimentation and progressive burial or overburden provides significant pressure and temperature. When these humic precursors are subjected to sufficient temperature and pressure for sufficient geologic time, they begin to undergo maturation process and present certain specific changes. Figure 1 shows the SEM images of three kerogen features defined as “solid,” “pendular,” and “spongy” by Walls and Diaz (2011), respectively, corresponding to immature, mature, and overmature stages.

The immature stage is considered to be the starting point from which thermal maturation transforms the solid kerogen to the other forms (Walls and Sinclair, 2011). Immature kerogen solids are composed of a heterogeneous mix of large molecules that are stable at low temperatures. Generally, the environment at the site of deposition of the organic matter controls the

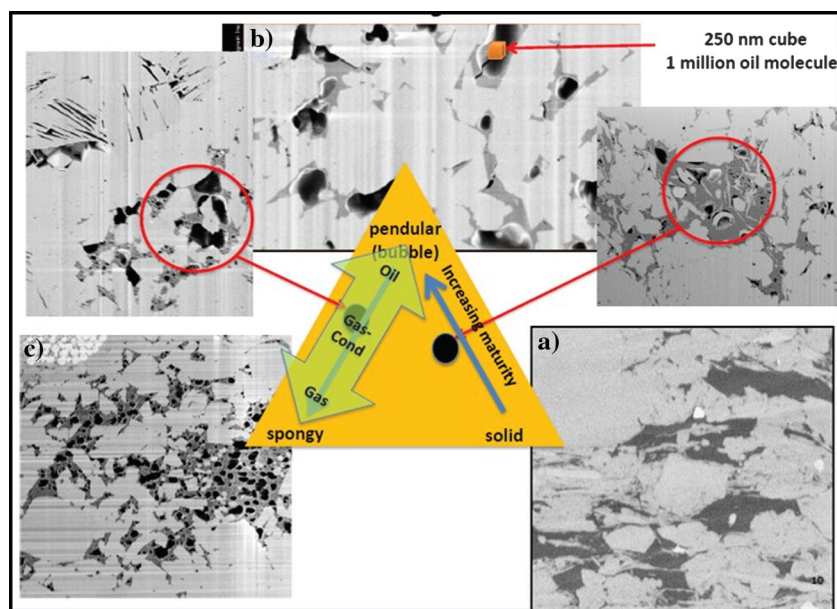


Figure 1. Diagram of three primary organic matter morphologies that are observed in hydrocarbon-bearing shales at different maturity stages (taken from Walls and Diaz, 2011): (a) immature, (b) mature, and (c) overmature. As shown in the lower right corner, the nonporous organic components (likely kerogen) correspond to the immature stages. At the peak of the triangle is the pendular organic material that is more common at mature stages, leaving kerogen-related porosity filled with oil. In the lower left corner is porous or spongy organic material as is commonly encountered in thermally overmature gas shales. Areas circled in red show combinations of the three basic forms.

quantity and quality of the kerogen found in organic shales. From a geologic perspective, the kerogen solids are deposited at the same time as the inorganic mineral grains. Then, they together undergo initial sedimentation, dehydration, compaction, and cementation. Therefore, during the geologic time of immature stages, the kerogen solids, along with other fine-grained inorganic particles, are load bearing and together contribute to the stiffness of the overall organic shale. As shown in Figure 1a, at immature stages, kerogen solids appear to surround inorganic mineral grains. Thus, the solid kerogen particles must be treated as a prominent part of the framework, and they play the similar role as the load-bearing silicate mineral matrix (Ahmadov, 2011; Walls and Sinclair, 2011; Zargari et al., 2013).

With progressive exposure to higher temperature, kerogen will breakdown into smaller molecules, some of which are precursors to oil, and in turn, its mass, solid volume, and hydrogen fraction decrease. At mature stage, with the transformation to oil, the residual kerogen is prone to be more aromatic, and its solid structure becomes more ordered and denser with stacks of aromatic sheets (Tissot et al., 1974; Derbyshire, 1991). As shown in Figure 1b, kerogen particles are connected with matrix and hence still play a load-bearing role. Meanwhile, the kerogen-related pores are generated due to the thermal conversion of kerogen to oil. Those maturation-produced intraparticle pores in kerogen do not collapse even in stress-bearing conditions, which are actually very similar to the secondary pores due to dissolution in carbonates.

As temperature keeps increasing and rocks get more mature, the oil is converted to gas through the process of thermal cracking. During this conversion, the volume of pore fluid increases, and this often causes overpressure in organic shales due to its extremely small permeability (Luo and Vasseur, 1996; Vernik and Landis, 1996; Yenugu and Han, 2013). At the overmature stage, as shown in Figure 1c, organic matters tend to exhibit spongy texture and are dispersed in the inclusion space of organic shale. Indeed, organic matter becomes more inclusion filling and the matrix is more supported by inorganic grains at overmature stages (Vernik and Nur, 1992; Ahmadov, 2011; Zargari et al., 2013). Note that, at the overmature stages, we use the term *inclusion space* (Zhu et al., 2012) to indicate the space occupied by mixture of fluids and organic matter solids. This is to avoid the confusion of *pore space*, which is commonly used for the fluid-filled pores.

The geochemical properties of kerogen change with maturation because it releases volatiles, such as CH<sub>4</sub>, CO<sub>2</sub>, and H<sub>2</sub>O, during thermal decomposition (Tissot et al., 1974). Thus, the solid structures of kerogen become denser and generally give rise to an increase in the density and moduli of kerogen solids (Okiongbo et al., 2005; Alfred and Vernik, 2012). At the overmature stage, continuous maturation of kerogen often leads to a rearrangement of the polyaromatic network and in turn, an extensive graphitization of residual kerogen can significantly stiffen the organic matter. To illustrate the representative changes concerning the role of kerogen upon maturation, Figure 2 shows the time-lapse SEM im-

ages of an organic shale sample before and after pyrolysis experiments. As we can see, not only the physical state of organic matter alters upon thermal maturation (Tissot et al., 1974), but also, and more importantly, the manners of the interaction between the inorganic and organic components experience a remarkable change — the organic matter gradually transforms from the role of load bearing to inclusion infillings.

## MODEL DEVELOPMENT

### Modeling workflows

It is clear that thermal maturation strongly changes the physical properties of organic-rich shales and therefore influences their effective elastic responses. We have to bear in mind that the observations regarding organic matter maturation, as mentioned in the previous section, must be taken into account when selecting appropriate rock-physics models to capture the elastic characteristics of organic shale.

As shown in Figure 3, a typical organic shale is composed of inorganic minerals (mainly clay and nonclay minerals) and organic matter, along with pore space between these components. The porosity in the organic shale can be divided into two parts: (1) matrix porosity  $\phi_{matrix}$  that are present in the inorganic part and (2) kerogen-related porosity  $\phi_{kerogen}$  that are produced due to thermal maturation. Kerogen-related porosity is considered to dominate the hydrocarbon storage capacity in organic shale. The matrix porosity is again partitioned into clay pores with bound water and nonclay pores with mobile water, using the method proposed by Xu and White (1995):

$$\phi_{clay} = V_{clay}\phi_{matrix}, \quad \phi_{nonclay} = \phi_{matrix} - \phi_{clay} \quad (1)$$

where  $V_{clay}$  is the clay volume that is normalized by the total volume of inorganic matrix. The schematic of modeling strategy for

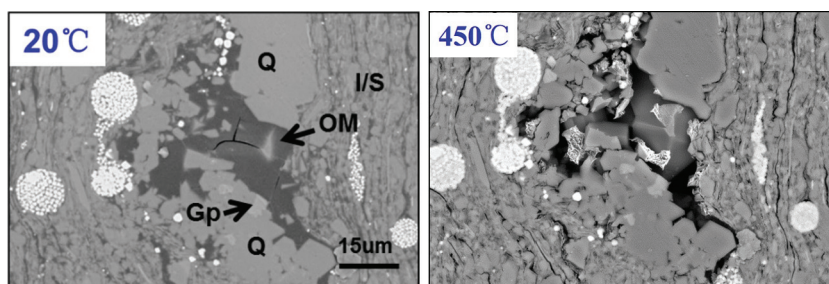


Figure 2. The SEM image of the organic shale (a) before and (b) after pyrolysis experiments. It is observed that the organic matters (denoted as OM) appear to surround inorganic mineral grains at 20°C. However, there exists significant grain boundary cracking between the inorganic and organic body when heating up to 450°C ( $R_o \sim 2.0$ ), and organic matters are more like inclusion-filling materials at the overmature stages.

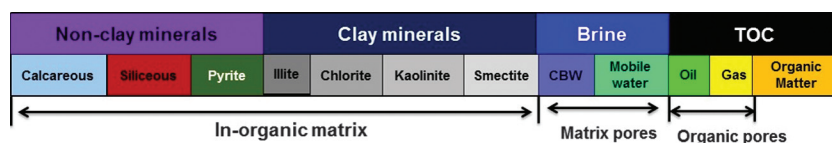


Figure 3. Schematic of the composition of organic-rich shales. Clay-bound water = CBM.

organic shale at different maturity stages is portrayed in Figure 4. The modeling framework is basically to answer two questions: (1) How do we describe the effective elastic properties of inorganic matrix frame? and (2) How do we add the organic matter in the former inorganic shale background upon kerogen maturation? The detailed modeling steps are given below:

- 1) We start by generating anisotropic clay structures. Clay mineral particles are featured as typical hexagonal symmetry that contains five independent elastic constants. Here, we assume the values of stiffnesses tensor components of clay as (Sayers, 2013)  $C_{11} = 44.9$  GPa,  $C_{33} = 24.2$  GPa,  $C_{44} = 3.7$  GPa,  $C_{66} = 11.6$  GPa, and  $C_{13} = 18.1$  GPa. Note that those elastic stiffnesses already represent the effect of clay micropores with bound water.
- 2) Silt-sized minerals (quartz, calcite, and pyrite) tend to exist as roughly spherical shapes that are randomly oriented, and their concentrations vary locally in unconventional shale plays. From a geologic perspective, those silt-sized minerals might be present in various forms due to differences in depositional environments and diagenetic processes (Hart et al., 2013). For example, calcite can be dispersed in a siliciclastic matrix or recrystallized to form coarse carbonate crystals. Moreover, calcite can also act as cementing component, enforcing rocks to resist shear deformation significantly. For simplicity, we can use anisotropic SCA (Hornby et al., 1994) to include quartz/feldspar, calcite/dolomite, and nonclay pores of matrix in the fully aligned clay to obtain the effective anisotropic elastic stiffness of inorganic matrix frame  $C_{\text{matrix}}$  because it is unnecessary to identify one of the minerals as the host and the other as inclusions. The effective stiffness tensor in the SCA model, yielding the effective estimate through mixing all phase in an iterative manner, can be expressed as (Hornby et al., 1994; Bandyopadhyay, 2009)

$$\sum_{r=1}^N v_r (\mathbf{C}^r - \mathbf{C}^{\text{SCA}}) [1 + \hat{\mathbf{G}} (\mathbf{C}^r - \mathbf{C}^{\text{SCA}})]^{-1} = 0, \quad (2)$$

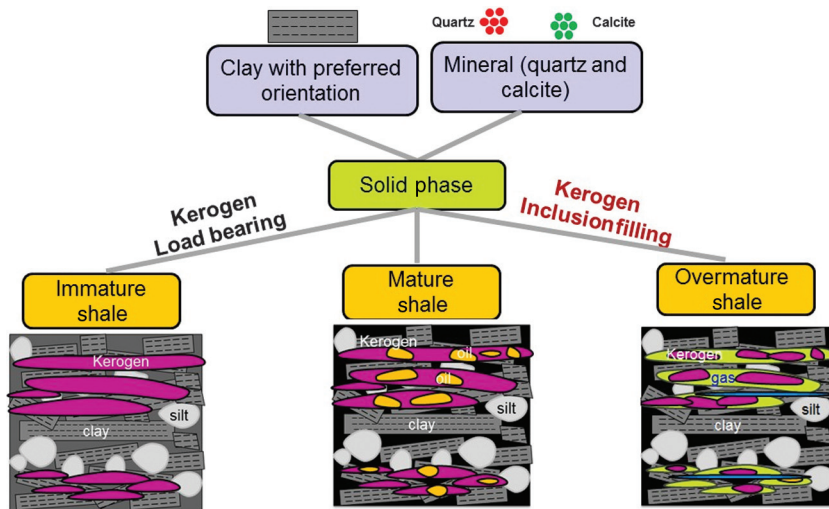


Figure 4. Conceptual diagram of rock-physics modeling in organic shale at different maturity stages.

where  $v_r$  is the volume fraction of  $r$ th constituent ( $r = 1, 2, \dots, N$ ) for the inorganic component of shale matrix,  $\mathbf{C}^r$  represents the stiffness tensor of the  $r$ th constituent,  $\mathbf{C}^{\text{SCA}}$  indicates the self-consistent effective elastic stiffness of inorganic matrix, and  $\hat{\mathbf{G}}$  is a fourth-rank tensor given by the strain Green's function integrated over the inclusion shape (Mura, 1987)

$$\hat{\mathbf{G}} = \frac{1}{8\pi} [\bar{\mathbf{G}}_{ijkl} + \bar{\mathbf{G}}_{jikl}]. \quad (3)$$

The nonzero components of  $\bar{\mathbf{G}}_{ijkl}$  for a transversely isotropic system are given by Mura (1987). Here, the aspect ratio of non-clay pores of matrix is set as 0.25, which is a typical value for interparticle pores (Xu and White, 1995; Zhao et al., 2013). Note that the nonclay pores are considered as inclusions with brine because shale matrix is not subject to Gassmann's fluid substitution routine due to its incapability of satisfying the conditions of pore-pressure equilibration.

- 3) The next step is to include the organic matter in the inorganic shale background. Organic matter is of particular interest not only because of its unique elastic characteristics but also due to the different manners in which it interacts with inorganic frame at different maturity stages. Consequently, as shown in Figure 4, we select different effective medium theories to handle organic matter's contribution to the overall elastic responses of organic shale as mentioned below.

#### Immature shale

At the immature stage, we presume that kerogen solids play the role of load bearing and serve as part of shale matrix. They tend to be laminated with elongated kerogen particles (Vernik and Landis, 1996; Vernik and Liu, 1997; Ahmadov, 2011); therefore, we can use Backus averaging theory to include the contribution of layered kerogen on the overall elastic properties of organic shale. Anisotropic Backus averaging theory gives a transversely isotropic equivalent medium described by five effective stiffnesses (Backus, 1962; Mavko et al., 2009):

$$\begin{aligned} C_{11}^* &= \langle C_{13}/C_{33} \rangle^2 / \langle 1/C_{33} \rangle \\ &\quad - \langle C_{13}^2/C_{33} \rangle + \langle C_{11} \rangle \\ C_{33}^* &= \langle 1/C_{33} \rangle^{-1} \\ C_{13}^* &= \langle C_{13}/C_{33} \rangle / \langle 1/C_{33} \rangle \\ C_{44}^* &= \langle 1/C_{44} \rangle^{-1} \\ C_{66}^* &= \langle C_{66} \rangle, \end{aligned} \quad (4)$$

where  $\langle \cdot \rangle$  indicates averages of the enclosed properties weighted by their volumetric proportions. As an example,  $\langle C_{11} \rangle = V_{\text{kerogen}} C_{11}^{\text{kerogen}} + (1 - V_{\text{kerogen}}) C_{11}^{\text{matrix}}$ , where  $V_{\text{kerogen}}$  is the volume fraction of kerogen and  $C_{11}^{\text{kerogen}}$  is the stiffness of kerogen at immature stages. The yielded vertically transverse isotropy (VTI) characteristics mainly depend on the contrast between the elastic properties of inorganic background and the kerogen itself.

### Mature shale

At the mature stage, by assuming the kerogen-related pores generated by thermal maturation as inclusions in the solid kerogen, we first use anisotropic DEM theory to obtain the effective elastic stiffnesses of porous kerogen. Then, to compute the overall elastic responses of organic shale, we still use the Backus averaging theory to handle the component of the porous kerogen. In the DEM, a small amount of inclusions of one phase is incrementally added to a background host medium in an iterative fashion. The process is continued until the desired proportion of the constituents is reached. The change in effective elastic stiffness  $dC$  due to an increase in  $dv$  is (Nishizawa, 1982; Hornby et al., 1994; Xu, 1998)

$$\frac{d}{dv}(\mathbf{C}^{\text{DEM}}(v)) = \frac{1}{1-v}(\mathbf{C}^{\text{fluid}} - \mathbf{C}^{\text{DEM}}(v)) \times [\mathbf{I} + \hat{\mathbf{G}}(\mathbf{C}^{\text{fluid}} - \mathbf{C}^{\text{DEM}}(v))]^{-1}, \quad (5)$$

where  $\mathbf{C}^{\text{fluid}}$  denotes the stiffness of hydrocarbon filled in kerogen-related porosity and  $\mathbf{C}^{\text{DEM}}(0)$  represents the stiffness of the solid kerogen.

### Overmature shale

At the overmature stage, organic matter particles have a semblance of flow texture and tend to suspend in the inorganic mineral components (Zargari et al., 2013). Therefore, it is reasonable to presume that organic matter is treated as a filling material of the inclusion space instead of the load-bearing matrix. Because the shear modulus of the organic-matter-fluid mixture is not zero, the solid substitution equation (Ciz and Shapiro, 2007) is used to capture the combined effect of the organic-matter-fluid mixture on the overall elastic properties of organic shale. The solid substitution equation is expressed in the compliance domain and given below:

$$\mathbf{s}_{ijkl}^{\text{sat}} = \mathbf{s}_{ijkl}^{\text{dry}} - \frac{(\mathbf{s}_{ijkl}^{\text{dry}} - \mathbf{s}_{ijkl}^0)(\mathbf{s}_{mnpq}^{\text{dry}} - \mathbf{s}_{mnpq}^0)}{[(\mathbf{s}^{\text{dry}} - \mathbf{s}^0) + (V_{\text{kerogen}} + \phi_{\text{kerogen}})(\mathbf{s}^{\text{mixture}} - \mathbf{s}^{\phi})]_{mnpq}}, \quad (6)$$

where  $\mathbf{s}_{ijkl}^{\text{dry}}$  is the fourth-rank effective elastic compliance tensor element of inorganic matrix,  $\mathbf{s}_{ijkl}^{\text{sat}}$  is the fourth-rank effective elastic compliance tensor of rock saturated with inclusion-filling material,  $\mathbf{s}_{ijkl}^0$  is the fourth-rank effective elastic compliance tensor of the solid mineral,  $\mathbf{s}^{\text{mixture}}$  is the effective compliance of inclusion-filling material mixed by hydrocarbons and dispersive kerogen particles, and  $\mathbf{s}^{\phi}$  is the compliance tensor of the inclusion space. Here,  $V_{\text{kerogen}}$  and  $\phi_{\text{kerogen}}$  represent the volume fraction of kerogen and kerogen-related porosity at the overmature stage, respectively.

The elastic compliance of dry rock can be calculated using the anisotropic DEM scheme. Note that the kerogen-fluid mixtures are not uniformly distributed and often considered to be patchy mixing. Thus, the effective modulus of kerogen-fluid mixture can be computed based on the Voigt average approximation (Domenico, 1976; Mavko et al., 2009):

$$K_{\text{mixture}} = V_{\text{kerogen}}/(V_{\text{kerogen}} + \phi_{\text{kerogen}})K_{\text{kerogen}} + \phi_{\text{kerogen}}/(V_{\text{kerogen}} + \phi_{\text{kerogen}})K_{\text{fluid}}, \quad (7)$$

$$G_{\text{mixture}} = V_{\text{kerogen}}/(V_{\text{kerogen}} + \phi_{\text{kerogen}})G_{\text{kerogen}} + \phi_{\text{kerogen}}/(V_{\text{kerogen}} + \phi_{\text{kerogen}})G_{\text{fluid}}, \quad (8)$$

where  $K_{\text{mixture}}$  and  $G_{\text{mixture}}$  denote the effective bulk and shear moduli of the kerogen-fluid mixture, respectively, and  $K_{\text{kerogen}}$  and  $G_{\text{kerogen}}$  denote the bulk and shear moduli of the organic matter at the overmature stage, respectively.

### Cautions for model applications

Regarding the applicability of the aforementioned workflow, several points listed below are of particular interest:

- 1) We have to bear in mind that the inputs of kerogen modulus for the rock-physics model vary upon maturation. Concerning with the specific organic shale reservoir, the elastic modulus of kerogen can be locally calibrated using atomic force microscopy, nanoindentation techniques, and other techniques (Zeszotarski et al., 2004; Ahmadov, 2011; Kumar, 2012; Yan and Han, 2013; Zargari et al., 2013). In addition, the inputs for fluids properties should also change locally at different maturity stages.
- 2) One of the essential assumptions of the inclusion-based theory is that the stress field inside the ellipsoid is considered to be uniform and not affected by the surrounding stress condition (Eshelby, 1957). Evidently, the inclusion theory is not appropriate to simulate kerogen's impact on the elastic responses of organic shale at the immature stage because kerogen solids serve as the load-bearing role and its stress state is certainly affected by the surrounding stress field of inorganic component. At the mature stage, the tiny kerogen-related pores created due to thermal maturation do not collapse and show "stiff" characteristics, which is considered to be somewhat independent of the surrounding stress-bearing conditions. Therefore, the inclusion theory is appropriate to characterize the impact of kerogen-related porosity on the overall elastic field.
- 3) An important conceptual difference between the DEM and SCA schemes is that the DEM scheme treats each constituent asymmetrically with a preferred host matrix, whereas the SCA scheme does not identify any specific host material but treats the composite as an aggregate of all the constituents (Mavko et al., 2009). Therefore, to mimic the elastic behavior of organic shale, we consider kerogen-related porosity due to the maturation and dissolution processes to resemble the physical realization of the DEM, whereas an aggregate of inorganic grain matrix may look more like a physical realization of SCA (Ruiz, 2009).
- 4) The modeling scheme assumes that the matrix pores and kerogen-related pores are isolated with respect to fluid flow, and in response, it simulates a high-frequency response for a fluid-saturated organic shale. Actually, shales have extremely low permeability and thus low fluid mobility, indicating that the pore pressure remains out of equilibrium, and rocks are necessarily in the unrelaxed status even in the typical seismic exploration-frequency band (Batzle et al., 2006; Zhao et al., 2015). This implies that for organic shale, seismic, sonic logging, and ultrasonic measurement may yield consistent velocity values (excluding issues with scattering effect).
- 5) In our modeling, clay platelets are assumed to be fully aligned and parallel to the bedding plane. However, the clay platelets vary in orientation but are aligned locally, and a considerable

portion of clay crystallinities is also randomly oriented. In general, the degree of alignment presents a wide range of dispersion and depends on the burial and compaction history (Kanitpanyacharoen et al., 2014). To compute the stiffness of an aggregate of partially aligned domains, we can average the elastic properties using the orientation distribution function suggested by Hornby et al. (1994), which can be derived from SEM image of the rock (Dræge et al., 2006; Bandyopadhyay, 2009).

- 6) Concerning the morphology of kerogen distribution, we often assume it has a lenticular shape with a continuous network in bedding-parallel direction (Vernik and Landis, 1996; Vernik and Milovac, 2011). However, the arrangement of kerogen may have dissimilar patterns, depending on its depositional environment as well as diagenesis. As displayed in Figure 5, the morphology of kerogen can be generally classified into two types: “lenses network” distribution and “scatter patches” distribution (Sone, 2012; Sone and Zoback, 2013). The lenses shape of kerogen tends to be spatially distributed in a continuous network, whereas kerogen with patches is prone to be distributed in an isolated pattern. Therefore, as introduced in the previous modeling schemes, for kerogen with lenses distribution, we can use the Backus averaging method to handle elastic contribution of solid kerogen. Nevertheless, when kerogen presents scatter patches distribution, such as other fine-grained mineral particles, we can use the Voigt-Reuss-Hill averaging method (Mavko et al., 2009) to take care of the impact of solid kerogen on the overall elastic field. Note that this is only applicable for the immature and mature shales.

## MODELING RESULTS AND ANALYSIS

### RPTs at different maturity stages

Using the approach outlined in the previous sections, we are able to construct the RPTs (Avseth et al., 2010), and thereby quantify the impact of geologic factors and reservoir parameters on the elastic responses of organic shale at different maturity stages. The parameters corresponding to each kerogen maturation stage are listed in Table 1.

The starting point in the modeling is a hypothetical immature shale, which has been well compacted with a matrix porosity of 0.10. As organic shale thermally matures because of the continuous compaction, the matrix porosity decrease to 0.07 at mature stages and 0.04 at overmature stages. The minerals in the organic shale consist of

20% clay, 20% carbonate, and 60% quartz-feldspar (QF), and, hence, the shale model is considered to be silica rich. The elastic modulus and density of mineral components used for calculations are listed in Table 2. One of the impediments to construct the RPTs is to establish the correlation between kerogen content and kerogen-related porosity. Because the thermal transformations of liable kerogen tend to create and maintain kerogen-related porosity, it is expected that kerogen-related porosity is directly proportional to the kerogen content at mature and overmature stages (Loucks et al., 2009). Therefore, high local TOC is often considered as a critical factor to evaluate shale reservoir because it is largely associated with the hydrocarbon storage capacity. In our modeling, it is assumed that the ratio of organic matter content to the kerogen-related porosity is roughly 2:1 for mature

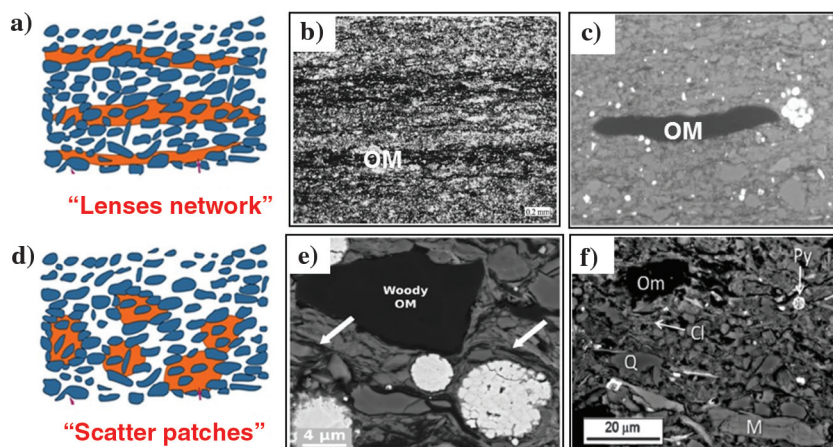
**Table 1. The related parameters to simulate RPTs for organic shale at immature, mature, and overmature stages, respectively. The elastic modulus of organic matter at the immature stage, mature stage, and overmature stage is reported by Yan and Han (2013), Qin et al. (2014), and Lucier et al. (2011), respectively.**

Maturity level	Hydrocarbon composition	$K_{\text{kerogen}}$ (GPa)	$G_{\text{kerogen}}$ (GPa)	$\rho_{\text{kerogen}}$ (g/cm <sup>3</sup> )	Matrix porosity
Immature	—	3.5	1.75	1.10	0.10
Mature	Oil	5	3.5	1.26	0.07
Overmature	Gas	7.98	4.18	1.34	0.04

**Table 2. Bulk modulus, shear modulus, and density for mineral components used in the calculations (references in Mavko et al., 2009).**

Mineral	Bulk modulus (GPa)	Shear modulus (GPa)	Density (g/cm <sup>3</sup> )
Quartz	37	44	2.65
Feldspar	37.5	15	2.62
Calcite	76.8	32.0	2.71
Dolomite	94.9	45.0	2.87

Figure 5. Examples of the morphology of OM distribution in organic shale: (a) conceptual model of lenses network, (b) photomicrographs in plain light showing laminated kerogen in low-porosity, tight black shale of the Bazhenov Formation (taken from Vernik and Landis, 1996), (c) back-scatter SEM photomicrographs of a Bakken Formation sample showing bedding-parallel kerogen lenses (taken from Ahmadov, 2011), (d) conceptual model of scatter patches, (e) woody organic matter showing scatter patches in immature organic shale of Stuart Ranges Formation (taken from Löhr et al., 2015), and (f) organic matter showing scatter patches in detrital-dominated mudstones of Cretaceous Mancos Shale (taken from Hart et al., 2013).



shale and 1:1 for overmature shale (Passey et al., 2010; Lucier et al., 2011; Modica and Lapierre, 2012). Note that this ratio is reservoir specific and should be locally calibrated with laboratory measurements and petrophysical analysis.

For simplicity, it is assumed that the kerogen-related porosity is saturated with oil at the mature stage and gas at the overmature stage (Luo and Vasseur, 1996). Note that the actual fluid phases are more complicated at the overmature stage: The earlier overmature stage mainly corresponds to the condensate-wet-gas window, whereas the later overmature stage primarily corresponds to the dry-gas window (Vernik and Landis, 1996). The aspect ratio of kerogen-related porosity at the mature and overmature stages is set as 0.4. The elastic modulus of kerogen at different maturity stages is reported by many authors (Zeszotarski et al., 2004; Ahmadov, 2011; Lucier et al., 2011; Kumar, 2012; Yan and Han, 2013; Zargari et al., 2013; Qin et al., 2014). The elastic modulus of kerogen at the immature, mature, and overmature stages is given in Table 1, respectively.

Using the proposed modeling schemes, the simulated elastic properties of the vertical (normal to the bedding plane)  $V_p/V_s$  ratio versus P-impedance for organic shale at the immature, mature, and overmature stages are displayed in Figure 6a–6c, respectively. As we can see, organic matter and mineralogical content can be considered two dominant factors affecting elastic responses of organic shale. As expected, for all three maturity stages, the QF contents increase organic shale's P-impedance, but significantly decrease its  $V_p/V_s$  ratio. This is predominantly caused by the elastic characteristics of quartz, which has a higher modulus and a much lower Poisson's ratio. In contrast, organic matter content tends to enhance the organic shale's elastic compressibility remarkably due to its unique characteristics of very low velocity and density. However, the relationships between  $V_p/V_s$  ratios and organic matter content are more complicated at different maturity stages. For immature shale, the  $V_p/V_s$  ratio decreases with organic matter concentrations for clay-rich shale, but exhibits a reversal trend for QF-rich shale. For mature shale, the  $V_p/V_s$  ratio generally decreases with organic matter content, and the sensitivity is more pronounced at low QF content. When the QF concentration is larger than 40%, the organic matter does not exercise an appreciable impact on  $V_p/V_s$  ratio. For overmature shale,  $V_p/V_s$  ratio shows a sharp decreasing trend with organic matter content at low- and high-QF contents, which is mainly attributed to the increasing kerogen porosity filled with gas. Overall, the impact of kerogen content on the elastic properties is relatively smaller than that of mineralogical constituents.

A key implication that can be drawn from the analysis above is that the impact of maturity level should be included when predicting elastic properties of organic shale. As illustrated in Figure 6, the vertical  $V_p/V_s$  ratio and P-impedance have different sensitivities to the variation in organic matter and mineralogical content at different maturity stages. This is of no surprise because the elastic responses are essentially controlled by the geologic mark overprinted by the thermal maturation process.

Generally, a potential sweet spot of organic shale reservoir is considered to have high QF content (high brittleness) and high TOC content (more kerogen-related porosity indicative of more storage capacity). Based on the above-mentioned RPTs analysis, higher TOC (corresponding to lower P-impedance) and higher QF content (corresponding to higher P-impedance) have a competing effect in determining P-impedance. Accordingly, it seems to be hard to identify sweet spots based on the mere interpretation of P-impedance. However, high TOC and high QF suggest a lower  $V_p/V_s$  ratio, especially for mature and overmature shales. That is to say, low

$V_p/V_s$  ratio anomalies can be potentially considered as seismic attributes for sweet-spot indicators. This finding can be helpful when applying RPTs to interpret acoustic-log data and prestack seismic inversion results.

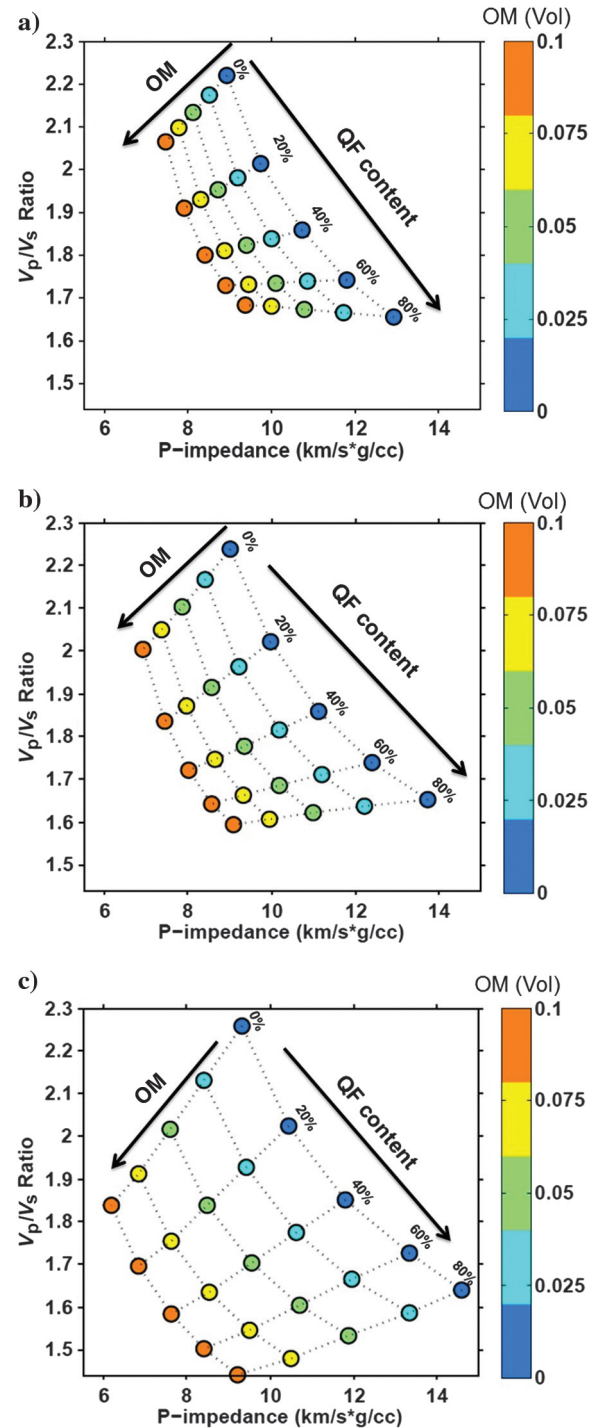


Figure 6. The RPTs of vertical P-impedance versus  $V_p/V_s$  ratio for varying QF content and volume fraction of TOC in organic shale at different maturity stages: (a) immature, (b) mature, and (c) overmature. The carbonate content is set as 20%, and the dots are color coded by volume fraction of TOC.

## Elastic anisotropy characteristics

Understanding elastic anisotropy characteristics in organic shale is needed for accurate seismic imaging, precise well ties, and proper interpretation of seismic data (Sayers, 2013). The source of the intrinsic anisotropy in organic shale is inherently complex and diffi-

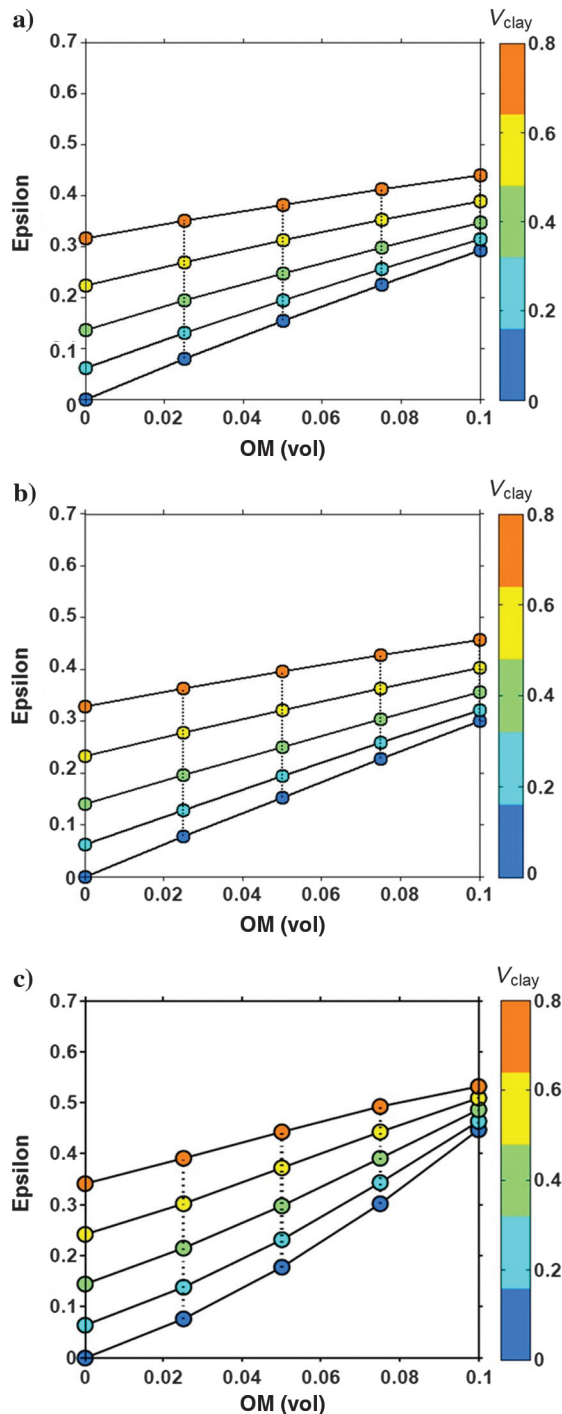


Figure 7. Comparisons of P-wave anisotropy parameter epsilon as a function of TOC (vol) at different maturity stages: (a) immature, (b) mature, and (c) overmature. The carbonate content is set as 20%, and the dots are color coded by volume fraction of clay content.

cult to discriminate arising from the coexistence of the organic and inorganic components. The purpose of this section is to analyze the causes of elastic anisotropy characteristics at different maturity stages through rock-physics modeling.

Figure 7 illustrates the influences of kerogen content and clay content on the P-wave velocity anisotropy as represented by the Thomsen parameter  $\epsilon$  for immature, mature, and overmature shales, respectively. As expected, for all organic shales at different maturity stages, the magnitude of elastic anisotropy increases with kerogen content. When the volume fraction of kerogen content is small, the elastic anisotropy is basically dominated by the clay alignment. With a larger volume fraction of clay, organic shale exhibits stronger anisotropy. Moreover, the sensitivity of elastic anisotropy to organic matter content decreases with an increase of clay content. This is mainly because the elastic properties' contrast of organic to inorganic component of shale is getting smaller as the volume fraction of clay is getting larger. The numerical results are also consistent with the geologic observation that the lamellar distribution of organic matter and compaction-induced preferred orientation of clay platelets significantly contribute to the intrinsic anisotropy of organic shale (Bandyopadhyay, 2009; Sayers, 2013; Kanitpanyacharoen et al., 2014). Next, we can compare the elastic anisotropy characteristics of organic shale at different maturity stages. For the given volume fraction of organic matter, the magnitude of  $\epsilon$  for overmature shale is slightly higher than that of mature and immature shales. This is mainly attributed to the increase in organic porosity due to hydrocarbon expulsion. Moreover, as shown in Figure 7c, for overmature shale, the sensitivity of elastic anisotropy to clay content is trivial at large volume fraction of organic matter content.

S-wave anisotropy as represented by the Thomsen parameter  $\gamma$  as a function of organic matter content for immature, mature, and overmature shales is displayed in Figure 8. The overall positive trend of S-wave anisotropy with kerogen and clay content remains unchanged. However, the sensitivity of  $\gamma$  to variations in kerogen is pronounced merely when clay content is relatively low. The effect of clay and kerogen contents on the anisotropic parameter  $\delta$  at different maturity stages is shown in Figure 9. The immature shale exhibits a negative  $\delta$  when clay content is zero, whereas the magnitude of  $\delta$  still increases with organic matter concentration. Generally, the overmature shale gives a particularly higher estimate of  $\delta$  than that predicted for immature and mature shales. In Figure 9c, for overmature shale, we also observe that when organic matter content is smaller than 2%, higher clay content tends to have higher  $\delta$ . Nevertheless, it exhibits a reverse trend when organic matter content is more than 2%; higher  $\delta$  corresponds to lower clay content. This is mainly because clay minerals' alignment dominates the magnitude of  $\delta$  when the volume fraction of organic matter is relatively small, whereas the  $\delta$  anisotropy is largely attributed to the inclusion space occupied by organic matter-gas mixture when organic matter content is relatively high.

## APPLICATIONS

In the following, we will use various RPTs to quantitatively analyze several sets of ultrasonic velocity and log data from different shale reservoirs. All the RPTs will be reservoir (basin) specific to honor the local geologic factors.

Lab ultrasonic data with different maturity level

We apply the theoretical framework described above to quality-controlled ultrasonic velocity and anisotropy measurements on a

variety of hydrocarbon organic shales, which are primarily based on publications by Vernik and Nur (1992), Vernik (1993), Vernik and Landis (1996), and Vernik and Liu (1997). The database also includes the information of mineralogy content, TOC, porosity, and

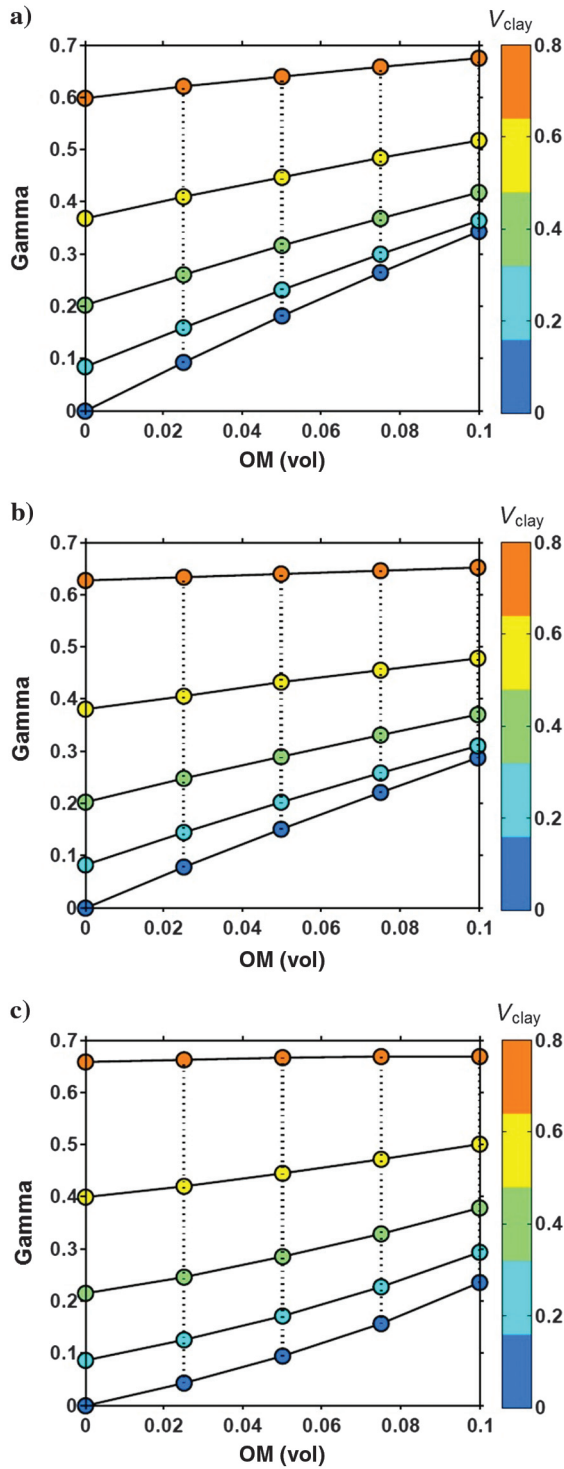


Figure 8. Comparisons of S-wave anisotropy parameter gamma as a function of TOC (vol) at different maturity stages: (a) immature, (b) mature, and (c) overmature. The carbonate content is set as 20%, and the dots are color coded by volume fraction of clay content.

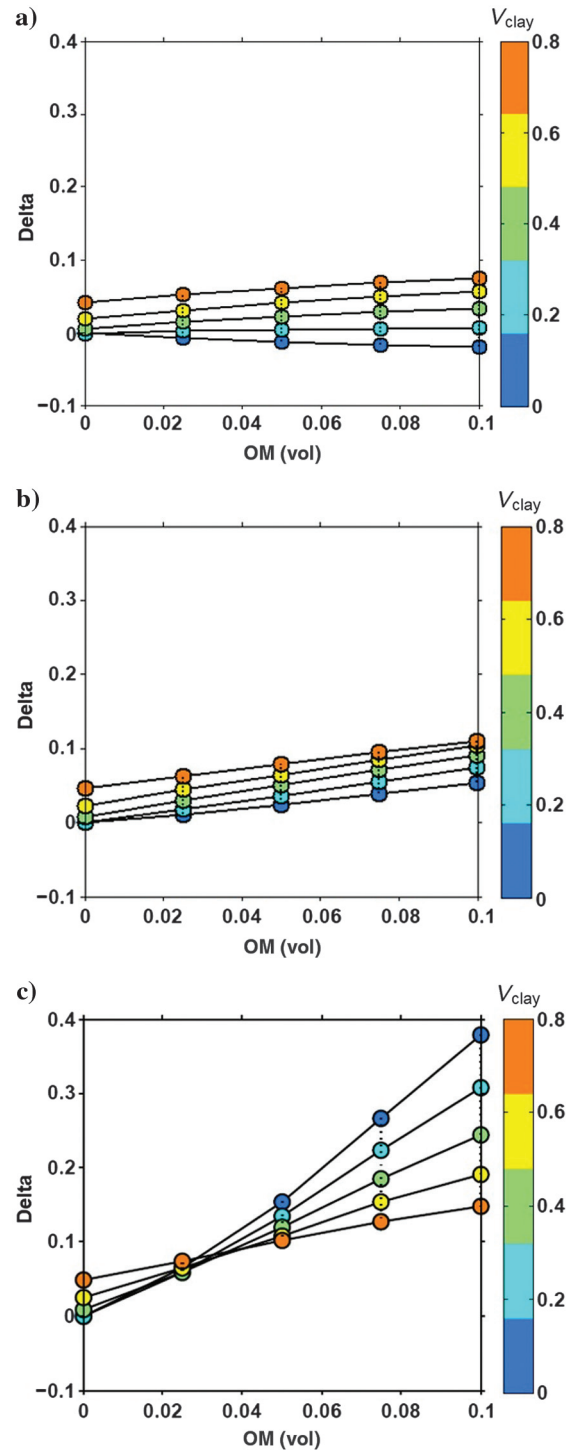


Figure 9. Comparisons of Thomsen's anisotropic parameters delta as a function of TOC (vol) at different maturity stages: (a) immature, (b) mature, and (c) overmature. The carbonate content is set as 20%, and the dots are color coded by volume fraction of clay content.

Downloaded 08/07/16 to 111.187.83.36. Redistribution subject to SEG license or copyright; see Terms of Use at http://library.seg.org/

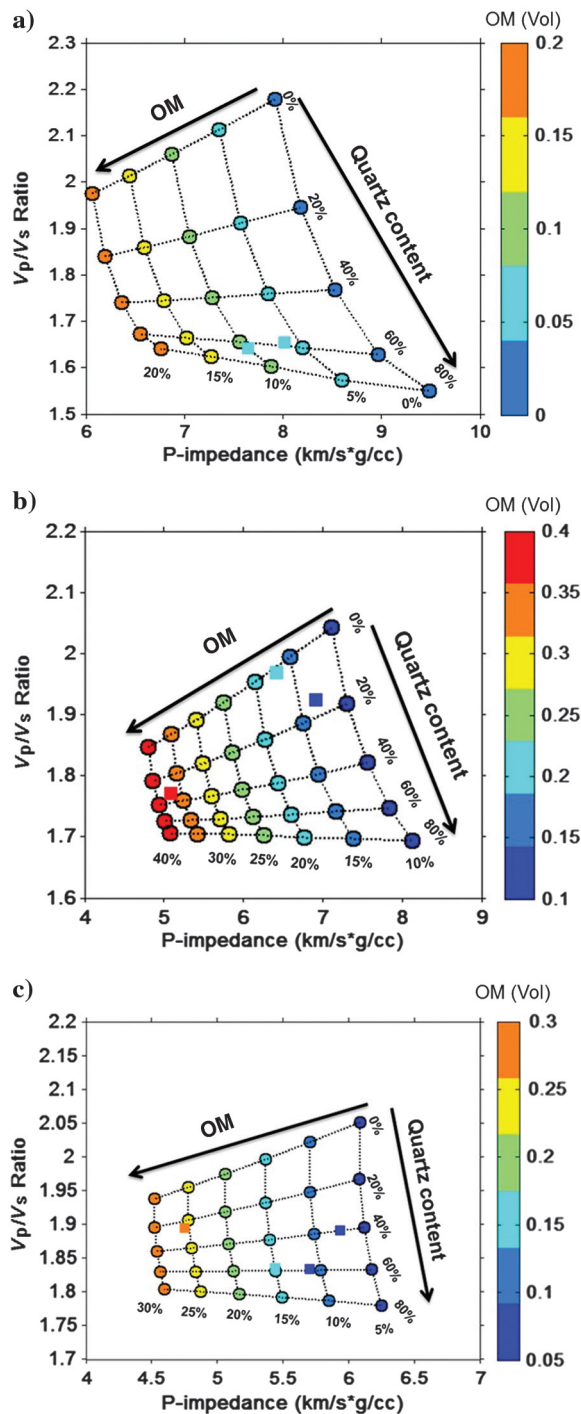


Figure 10. Rock-physic interpretation of lab data based on RPT of immature shale. The data superimposed on the immature RPT are from the Monterey Shale with low-rank  $R_o$  ranging from 0.42 to 0.44. The matrix porosity depicted in panel (a) is set as 0.10, and the two samples have porosities of 11.4% and 10%, respectively. The matrix porosity in panel (b) is set as 0.20, and the three samples have porosities of 21%, 21%, and 18%, respectively. The matrix porosity in panel (c) is set as 0.30, and the four samples have porosities of 28.8%, 30.9%, 29.6%, and 29.3%, respectively. The carbonate content is set as 0.20, and the QF content ranges from 0% to 80%. The data are color coded by the volume fraction of organic matter.

maturity level, which are characterized and quantified from XRD mineralogy, Rock-Eval organic geochemical analysis, vitrinite reflectance, and SEM observations.

Figure 10 displays RPT of vertical P-impedance versus  $V_p/V_s$  ratio for immature shale, superimposed with data from Monterey Shale having  $R_o$  (%) from 0.42 to 0.44. The typical lithologies of the middle Miocene Monterey Shale (California) include QF, clay, opal, and carbonate, with a wide range of porosity from 0.10 to 0.30. To better understand the effect of matrix porosity and to highlight the impact of mineralogy and organic matter content, we make three RPTs of immature shale with matrix porosities of 0.10, 0.20, and 0.30, respectively. The template basically shows a good agreement with the scarce data points and clearly suggests that organic matter has a significant impact on P-impedance. In addition, comparisons of the Figure 10a–10c convey the message that the calibration of matrix porosity is important for using RTPs to interpret a velocity data set.

As shown in Figure 11, the mature RPT is applied to the tight Mississippian–Devonian Bakken Shale, with  $R_o$  (%) ranging from 0.61 to 1.19, which typically falls within the mature oil window. The RPT indicates that the mineralogical content of Bakken Shale is predominated by QF content, which is indeed consistent with the XRD analysis (Vernik and Liu, 1997). In addition, the good alignment of data clusters along the constant organic matter content lines clearly suggests that the modeling framework can correctly capture the effect of organic matter on the elastic responses of organic shale. Figure 12 displays the overmature RPT superimposed with data from Niobrara Shale with  $R_o$  (%) ranging from 1.31 to 1.46. The lithology of the Upper Cretaceous Niobrara Formation is marls mainly composed of silt and carbonate. The overmature RPT indicates that most of the data points sit within a narrow range of organic matter content from 2.5% to 5%, and the fluctuations of P-impedance and  $V_p/V_s$  ratio are mainly attributed to the variation in mineralogical content.

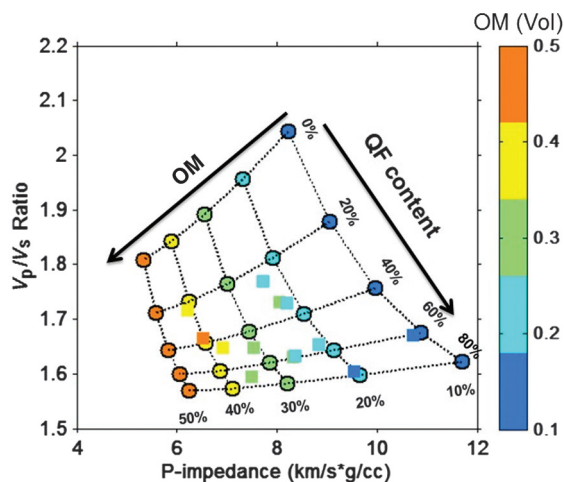


Figure 11. Rock-physic interpretation of lab data based on RPT of mature shale. The data superimposed on the mature RPT are from the Bakken Shale with low-rank  $R_o$  ranging from 0.61 to 1.19. The matrix porosity is set as 0.02, and the carbonate content is set as 20%. The TOC content ranges from 10% to 50%, and the QF content ranges from 0% to 80%. The data are color coded by volume fraction of TOC.

Log data from Barnett Shale gas reservoir

The study area is from the high-thermal-maturity Barnett Shale gas reservoir in the Fort Worth basin. A crossplot of P-impedance versus  $V_p/V_s$  ratio template superimposed with log data from Barnett Shale Formation is displayed in Figure 13. The petrophysical interpretation of mineralogical content is displayed on the right panel of the crossplot. Clearly, the Barnett Shale reservoir formation is predominantly siliciclastic mixtures of quartz and clay, with relatively low carbonate and little pyrite content. Based on the well-log analysis, the average matrix porosity is set as 0.05 and the carbonate content is set as 0.2 for constructing the overmature RPT. The overmature model predictions using appropriate ranges of TOC and QF content roughly describe the

data cloud. According to our RPT, the logging data can be interpreted to have TOC ranging from 4% to 8% and QF content ranging from 40% to 60%, which is consistent with the petrophysical analysis of the logging data. Note that the data are very scattered, and some data points with lower TOC even show smaller P-impedance and lower  $V_p/V_s$  ratio than that with higher TOC. This suggests that other factors, for instance, the variations in porosity and mineral content, might be responsible for this data scattering. Again, this illustrates that our RPT can provide reasonable interpretation for logging data in terms of TOC and mineralogical content, which are considered to be crucial factors affecting reservoir quality evaluation.

Impact of kerogen distribution on anisotropy characteristics

The studied shale oil reservoir is from the Permian Lucaogou Formation of Jimsar Sag, which is located in the Xinjiang Oil Shale field, northwestern China. As shown in the ternary plot of Figure 14, the reservoir formations are predominantly composed of fine-grained clastic and carbonates rocks. The deposition environment is primarily associated with the microfacies of delta front distal bar and beach bar of shore shallow lake. The vitrinite reflectance (% Ro) is approximately 0.7–1.0, indicating mature oil window. As can be seen in Figure 15, the morphology of the kerogen is prone to exhibit scatter patches distribution, and some tiny kerogen-related pores due to thermal maturation are also observed in Figure 15c. Figure 16 shows the comparison of P-wave anisotropy  $\epsilon$  predicted by rock-physics modeling assuming kerogen with scatter patches and lenses network, respectively, superimposed with the measured ultrasonic data for organic shale samples from the studied reservoir. In this case, the porosity contribution on the elastic anisotropy is trivial because porosity of all samples ranges between 1% and 3%. As expected, Thomsen’s anisotropic parameter  $\epsilon$  predicted by scatter patches model has less sensitivity to kerogen variation. It is clear that the scatter patches model gives a good match with the measured data, whereas the lenses network model significantly overestimates the anisotropy magnitude of the samples. This

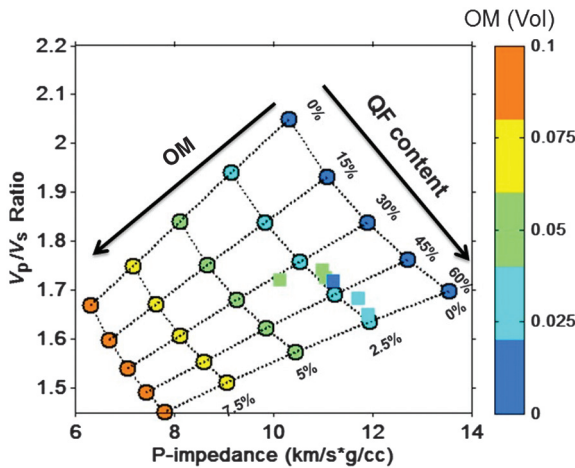


Figure 12. Rock-physics interpretation of lab data based on RPT of overmature shale. The data superimposed on the mature RPT are from the Niobrara Shale with low-rank Ro ranging from 1.15 to 1.46. The matrix porosity is set as 0.06, and the carbonate content is set as 40%. The TOC content ranges from 0% to 10%, and the QF content ranges from 0% to 80%. The data are color coded by volume fraction of TOC.

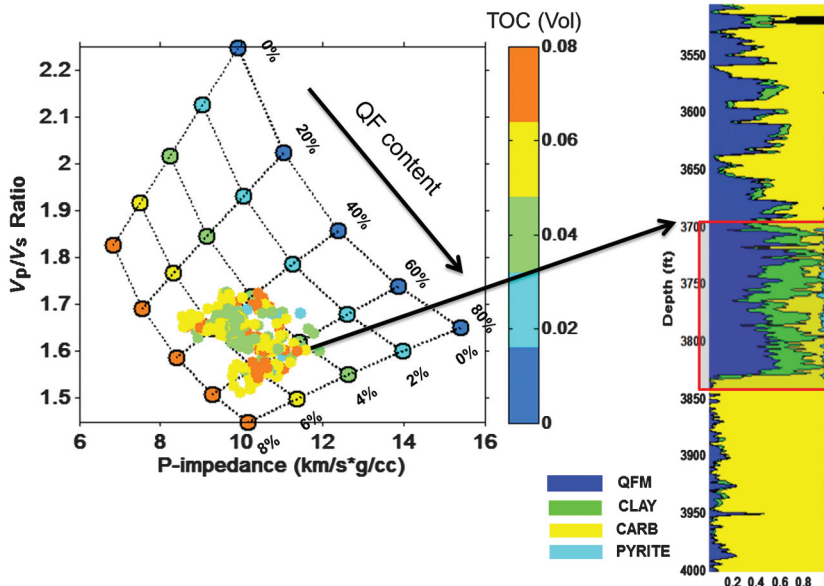


Figure 13. Rock-physics interpretation of log data based on RPT of overmature shale. All of the data points are from the well-log data of the Barnett Shale gas reservoir in the Fort Worth Basin, which are color coded by the volume fraction of TOC. The figure on the right panel is a petrophysical analysis of mineralogical content as a function of depth, in which the shadow zones indicate the depth range of Barnett Shale reservoir. The average matrix porosity is set as 0.06, and the carbonate content is set as 0.2 for constructing the overmature RPT.

Downloaded 08/07/16 to 111.187.83.36. Redistribution subject to SEG license or copyright; see Terms of Use at http://library.seg.org/

suggests that the elastic anisotropy characteristics in organic shale not only depend on the kerogen content and clay platelets but also depend on the morphology of kerogen distribution. Moreover, as we can observe from the anisotropy measurement color coded by volume fraction of clay content, given the kerogen content, the higher the clay content, the higher the anisotropy magnitude. This is also roughly consistent with our modeling results.

DISCUSSIONS

It is necessary to point out that the process of kerogen maturation, involving physical and chemical changes during millions of years at geologic time, is a continuous and highly nonlinear process. In addition, the complicated geologic processes and the statistical fluctuations in geologic history can cause organic shale to exhibit heterogeneities occurring at various extents. Concerning the role of organic matter in the inorganic background, the load-bearing organic matter and inclusion-filling organic matter might coexist in organic shale at certain maturity stages. There is not a clear boundary between different maturity levels, and there exists a transition process from immature to mature or from mature to overmature stages. As a

consequence, microstructural and textural properties of organic matter should vary in a continuous and chaotic manner upon kerogen maturation, rather than in an abrupt way as we simplify in the modeling schemes. To perform a first-order investigation of the impact of kerogen maturation on the elastic responses of organic shale, we

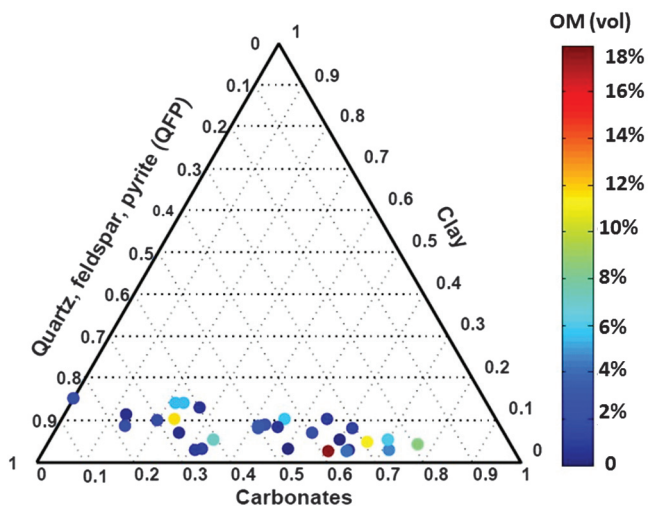


Figure 14. Ternary plot representation of the sample material composition from shale oil reservoir in the Xinjiang Oil Shale field, northwestern China. The data points are color coded by volume fraction of organic matter.

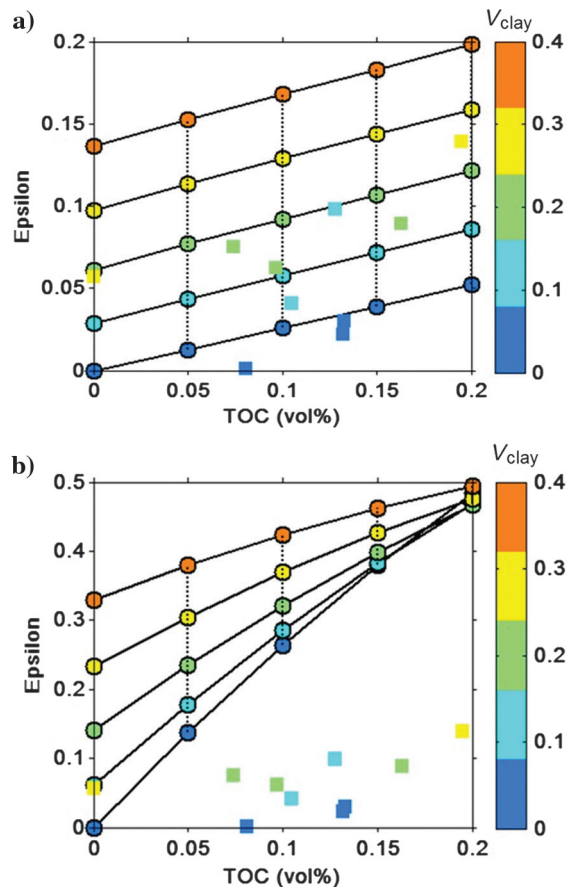


Figure 16. Comparisons of P-wave anisotropy parameter epsilon (core measurements) as a function of organic matter content (vol). Kerogen is assumed to have (a) scatter patches distribution and (b) lenses network distribution. The data points color coded by volume fraction of clay content are from the anisotropy measurement of the organic shale sample from the Xinjiang Oil Shale field, northwestern China.

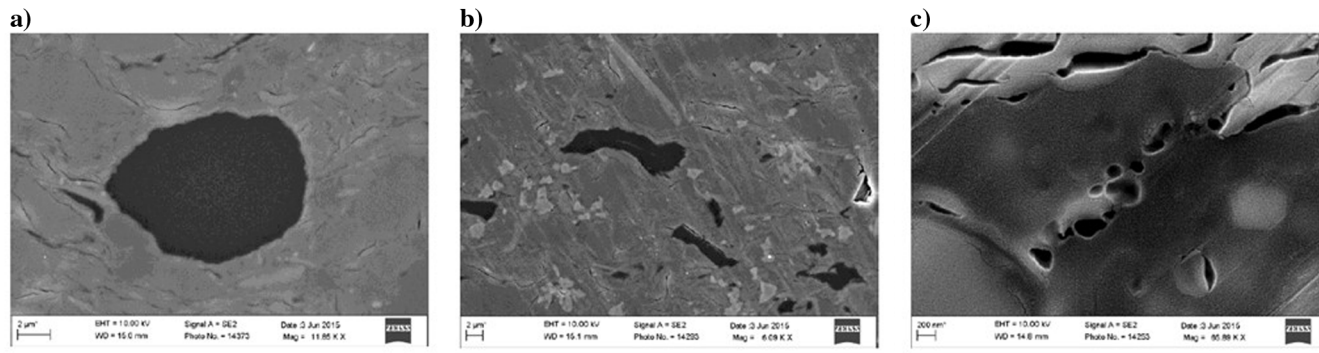


Figure 15. The SEM images from section of organic shale sample in the Xinjiang Oil Shale field, northwestern China.

purposely simplify the maturation processes into three main stages: immature, mature, and overmature, and therefore to capture their main evolution characteristics upon kerogen maturation.

Not only do the kerogen properties naturally vary upon maturation, the inorganic mineralogy composition change is also an inherent product of thermal alternation because temperature is commonly the key factor in dissolution and precipitation of some unstable minerals (Drøge et al., 2006). For example, with temperature increasing, smectite can react to form illite and quartz. Also, pyrite can be easily formed within organic shale when anoxic conditions are established. Given the unique elastic modulus of pyrite ( $K = 138.6$  GPa and  $G = 108.9$  GPa), the occurrence of pyrite within organic shale might potentially result in increased P-impedance and a decreased  $V_p/V_s$  ratio (Ahmadov, 2011). Regarding real application, the mineral constituents selection should be referenced to the XRD analysis and the petrophysical and image analysis. However, in our modeling framework, the mineralogical composition evolution at different maturity stages is ignored. In addition to the mineralogical composition, the degree of clay alignment also varies upon kerogen maturation.

In our modeling, we also make a few simplifications and assumptions to describe the microstructure of the organic shale containing complex multiphase material. For example, the water-filled nonclay matrix pores and hydrocarbon-filled kerogen-related pores are assumed to have ellipsoid shapes, and their aspect ratios are set as 0.25 and 0.4, respectively. However, in real organic shale, pore geometries often exhibit irregular microstructures and there certainly exists a distribution of pore-aspect ratios. SEM, TEM, and CT scanning can assist in characterizing and quantifying the microstructural features of organic shale. The impact of aspect ratio distributions of pores on elastic properties of shales has been investigated in detail by Vasin et al. (2013). Another issue is the consideration of matrix porosity, which might also bring uncertainty in determining the elastic responses of organic shales. In general, matrix porosity in most organic shale reservoirs is typically between 2% and 10% (Passy et al., 2010; Hart et al., 2013). At mature and overmature stages, most of the matrix porosity is lost due to the continuous physical and chemical compactions. At immature stages, the matrix porosity can span a wide range, depending on the depositional and burial history. Figure 17 shows the influence of

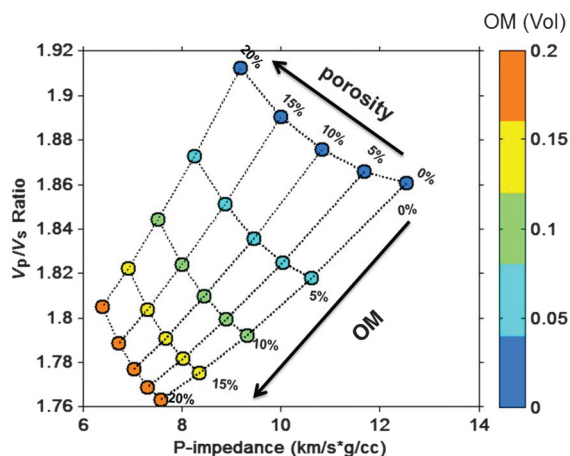


Figure 17. The effect of matrix porosity on the vertical P-impedance and  $V_p/V_s$  ratio of immature shale. The silica, carbonate, and clay contents are set as 0.4, 0.3, and 0.3, respectively.

matrix porosity on the elastic properties of immature shale. It is of no surprise that the matrix porosity reduces P-impedance and increases  $V_p/V_s$  ratio, and this effect is more pronounced for immature shale with lower organic richness.

Microcracks might be generated due to the hydrocarbon expulsion and geopressure evolution during the thermal cracking process (Vernik, 1993; Johnston and Christensen, 1995; Vernik and Landis, 1996; Allan et al., 2014; Yenugu, 2014). These microcracks might significantly aid primary hydrocarbon migration, particularly horizontally (Vernik and Landis, 1996). However, several authors (Zargari et al., 2013; Kanitpanyacharoen et al., 2014) also report that no significant cracks are generated after hydrous pyrolysis, which is to mimic the thermal maturation process. In our modeling approach for mature and overmature shales, we assume no microcracks are created or microcracks are closed at the in situ pressure condition. Generally, whether those microcracks remain open at depth depends on the in situ stress distribution, fracture toughness, pore pressure, and fluid expulsion/production (Allan et al., 2015). We can readily use anisotropic DEM theory to simulate the effect of microcracks on the overall elastic properties of organic shale. An aspect ratio of 0.01 is used to represent the microstructure of microcracks. Figure 18 shows the possible effect of subhorizontal microcracks

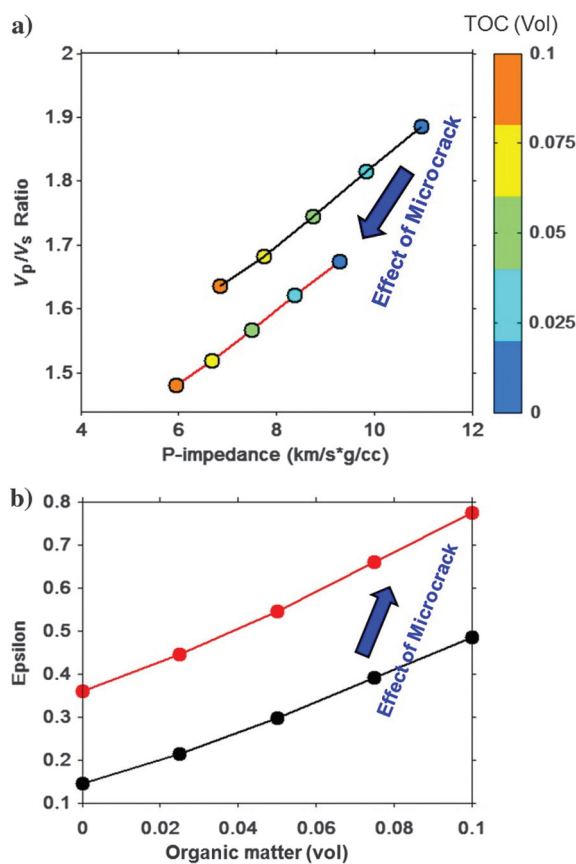


Figure 18. The effect of subhorizontal microcracks on the elastic responses and P-wave anisotropy characteristic of overmature shale: (a) vertical P-impedance and  $V_p/V_s$  ratio crossplot and (b) epsilon as a function of TOC. Red and black lines represent prediction including the effect of microcracks and without the microcracks, respectively. The average matrix porosity is set as 0.04. The carbonate and clay content is set as 0.2 and 0.2, respectively. The aspect ratio of microcrack is set as 0.01, and the crack density is set as 0.05.

on the overmature shale's elastic responses as well as its P-wave anisotropy characteristics. Clearly, the occurrences of microcracks cause vertical P-impedance and  $V_p/V_s$  ratio to decrease. Physically, this is understandable, because when the microcracks are dry or filled with gas, the seismic propagation P-wave velocity that is normal to the cracks will be dramatically decreased. Furthermore, as shown in Figure 18b, the magnitude of P-wave anisotropy is significantly enhanced by the overprint of microcracks. This is also in agreement with findings by Vernik and Landis (1996), who state that the strong elastic anisotropy in organic-rich shales is further enhanced due to the presence of bedding-subparallel microcracks in geopressed, thermally mature black shales that have undergone main-stage hydrocarbon generation and primary migration.

## CONCLUSIONS

On the basis of organic matter maturation processes, we present a framework to model elastic properties of organic shale at different maturity stages. Our new model incorporates the evolution of physical properties of organic shale during the course of thermal maturation. In particular, the interacting behavior of kerogen with mineral matrix is depicted through different approaches. Using the proposed modeling schemes, we are able to construct RPTs for immature, mature, and overmature shales, respectively. The modeling results suggest that, for the given matrix porosity, the TOC in combination with mineralogical composition primarily controls the elastic responses of organic shale. Vertical P-impedance and  $V_p/V_s$  ratio generally decrease with organic matter content, and, more importantly, such influences strongly depend on the maturity level. The developed model can also capture the correlation of organic shale's VTI anisotropy characteristics with organic richness as well as clay alignment. Furthermore, it is demonstrated that the morphology of kerogen distribution exercises a significant impact on the seismic anisotropies.

The calibration of the model with lab and well-logging data indicates that the modeling framework allows us to successfully capture the elastic characteristics of organic shale with different maturity levels, and therefore can be further used in amplitude variation with offset modeling/interpretation and reservoir characterization of shale reservoirs. The modeling framework presented here provides a general strategy to describe the elastic responses of organic shale. Nevertheless, regarding its application to specific shale reservoirs, we suggest it should be locally calibrated due to tremendous variability of reservoir properties and basin evolution environments.

## ACKNOWLEDGMENTS

This work was supported by Fluids and DHI consortium of the Colorado School of Mines and University of Houston, China National 973 Key Basic Research and Development Program (2014CB239006), the Foundation of State Key Laboratory of Shale Oil and Gas Enrichment Mechanisms and Effective Development, and Innovative Program of Shanghai Municipal Education Commission.

## REFERENCES

- Ahmadv, R., 2011, Microtextural, elastic and transport properties of source rocks: Ph.D. thesis, Stanford University.
- Alfred, D., and L. Vernik, 2012, A new petrophysical model for organic-rich shales: Presented at the SPWLA 53rd Annual Logging Symposium, 16–20.
- Allan, A. M., T. Vanorio, and J. E. P. Dahl, 2014, Pyrolysis-induced P-wave velocity anisotropy in organic-rich shales: *Geophysics*, **79**, no. 2, C73–C88, doi: [10.1190/geo2013-0254.1](https://doi.org/10.1190/geo2013-0254.1).
- Allan, A. M., W. Kanitpanyacharoen, and T. Vanorio, 2015, A multiscale methodology for the analysis of velocity anisotropy in organic-rich shale: *Geophysics*, **80**, no. 4, D41–D53, doi: [10.1190/geo2014-0192.1](https://doi.org/10.1190/geo2014-0192.1).
- Avseth, P., T. Mukerji, G. Mavko, and J. Dvorkin, 2010, Rock physics diagnostics of depositional texture, diagenetic alterations and reservoir heterogeneity in high porosity siliciclastic sediments and rocks — A review of selected models and suggested workflows: *Geophysics*, **75**, no. 5, 75A31–75A47, doi: [10.1190/1.3483770](https://doi.org/10.1190/1.3483770).
- Backus, G., 1962, Long-wave elastic anisotropy produced by horizontal layering: *Journal of Geophysical Research*, **67**, 4427–4440, doi: [10.1029/JZ067i011p04427](https://doi.org/10.1029/JZ067i011p04427).
- Bandyopadhyay, K., 2009, Seismic anisotropy: Geological causes and its implications to reservoir geophysics: Ph.D. thesis, Stanford University.
- Batzle, M. L., D. H. Han, and R. Hofmann, 2006, Fluid mobility and frequency-dependent seismic velocity — Direct measurements: *Geophysics*, **71**, no. 1, N1–N9, doi: [10.1190/1.2159053](https://doi.org/10.1190/1.2159053).
- Carcione, J. M., and A. F. Gangi, 2000, Gas generation and overpressure: Effects on seismic attributes: *Geophysics*, **65**, 1769–1779, doi: [10.1190/1.1444861](https://doi.org/10.1190/1.1444861).
- Carcione, J. M., H. B. Helle, and P. Avseth, 2011, Source-rock seismic-velocity models: Gassmann versus Backus: *Geophysics*, **76**, no. 5, N37–N45, doi: [10.1190/geo2010-0258.1](https://doi.org/10.1190/geo2010-0258.1).
- Carcione, J. M., and P. Avseth, 2015, Rock-physics templates for clay-rich source rocks: *Geophysics*, **80**, no. 5, D481–D500, doi: [10.1190/geo2014-0510.1](https://doi.org/10.1190/geo2014-0510.1).
- Ciz, R., and S. Shapiro, 2007, Generalization of Gassmann equations for porous media saturated with a solid material: *Geophysics*, **72**, no. 6, A75–A79, doi: [10.1190/1.2772400](https://doi.org/10.1190/1.2772400).
- Derbyshire, F., 1991, Vitrinite structure: alterations with rank and processing: *Fuel*, **70**, 276–284, doi: [10.1016/0016-2361\(91\)90113-O](https://doi.org/10.1016/0016-2361(91)90113-O).
- Dræge, A., M. Jakobsen, and T. A. Johansen, 2006, Rock physics modeling of shale diagenesis: *Petroleum Geoscience*, **12**, 49–57, doi: [10.1144/1354-079305-665](https://doi.org/10.1144/1354-079305-665).
- Domenico, S. N., 1976, Effect of brine-gas mixture on velocity in an unconsolidated reservoir: *Geophysics*, **41**, 882–894, doi: [10.1190/1.1440670](https://doi.org/10.1190/1.1440670).
- Eshelby, J. D., 1957, The determination of the elastic field of an ellipsoidal inclusion, and related problems: *Proceedings of the Royal Society of London, Series A: Mathematical and Physical Sciences*, **241**, 376–396.
- Guo, Z., X. Li, C. Liu, X. Feng, and Y. Shen, 2013, A shale rock physics model for analysis of brittleness index, mineralogy, and porosity in the Barnett Shale: *Journal of Geophysics and Engineering*, **10**, 025006–025011, doi: [10.1088/1742-2132/10/2/025006](https://doi.org/10.1088/1742-2132/10/2/025006).
- Hart, B. S., J. Macquaker, and K. G. Taylor, 2013, Mudstone (shale) depositional and diagenetic processes: Implications for seismic analyses of source-rock reservoirs: *Interpretation*, **1**, B7–B26, doi: [10.1190/INT-2013-0003.1](https://doi.org/10.1190/INT-2013-0003.1).
- Hornby, B. E., L. M. Schwartz, and J. A. Hudson, 1994, Anisotropic effective-medium modeling of the elastic properties of shales: *Geophysics*, **59**, 1570–1583, doi: [10.1190/1.1443546](https://doi.org/10.1190/1.1443546).
- Johnston, J. E., and N. I. Christensen, 1995, Seismic anisotropy of shales: *Journal of Geophysical Research*, **100**, 5991–6003, doi: [10.1029/95JB00031](https://doi.org/10.1029/95JB00031).
- Kanitpanyacharoen, W., T. Vanorio, Y. Liu, C. Benmore, and X. Xiao, 2014, Evolution of mineral fabrics and microstructures in Kimmeridge Shale upon kerogen maturation: 84th Annual International Meeting, SEG, Expanded Abstracts, 2783–2786.
- Kumar, V., 2012, Geomechanical characterization of shale using nano-indentation: M.Sc. dissertation, University of Oklahoma.
- Löhr, S. C., E. T. Baruch, P. A. Hall, and M. J. Kennedy, 2015, Is organic pore development in gas shales influenced by the primary porosity and structure of thermally immature organic matter?: *Organic Geochemistry*, **87**, 119–132, doi: [10.1016/j.orggeochem.2015.07.010](https://doi.org/10.1016/j.orggeochem.2015.07.010).
- Loucks, R. G., R. M. Reed, S. C. Ruppel, and D. M. Jarvie, 2009, Morphology, genesis, and distribution of nanometer-scale pores in siliceous mudstones of the Mississippian Barnett shale: *Journal of Sedimentary Research*, **79**, 848–861, doi: [10.2110/jsr.2009.092](https://doi.org/10.2110/jsr.2009.092).
- Lucier, A. M., R. Hofmann, and L. T. Bryndzia, 2011, Evaluation of variable gas saturation on acoustic log data from the Haynesville Shale gas play, NW Louisiana, USA: *The Leading Edge*, **30**, 300–311, doi: [10.1190/1.3567261](https://doi.org/10.1190/1.3567261).
- Luo, X., and G. Vasseur, 1996, Geopressing mechanism of organic matter cracking: Numerical modeling: *AAPG Bulletin*, **80**, 856–874.
- Mavko, G., T. Mukerji, and J. Dvorkin, 2009, *The rock physics handbook*: Cambridge University Press.
- Modica, C. J., and S.G. Lapierre, 2012, Estimation of kerogen porosity in source rocks as a function of thermal transformation: Example from the Mowry Shale in the Powder River Basin of Wyoming: *AAPG Bulletin*, **96**, 87–108, doi: [10.1306/04111110201](https://doi.org/10.1306/04111110201).
- Mura, T., 1987, *Micromechanics of defects in solid*: Martinus Nijhoff Pub.

- Nishizawa, O., 1982, Seismic velocity anisotropy in a medium containing oriented cracks: *Journal of Physics of the Earth*, **30**, 331–347, doi: [10.4294/jpe1952.30.331](https://doi.org/10.4294/jpe1952.30.331).
- Okiongbo, K. R., A. C. Aplin, and S. R. Larter, 2005, Changes in type II kerogen density as a function of maturity: Evidence from the Kimmeridge Clay Formation: *Energy and Fuels*, **19**, 2495–2499, doi: [10.1021/ef050194+](https://doi.org/10.1021/ef050194+).
- Passey, Q. R., K. M. Bohacs, W. L. Esch, R. Klimentidis, and S. Sinha, 2010, From oil-prone source rock to gas-producing shale reservoir — Geologic and petrophysical characterization of unconventional shale-gas reservoirs: Presented at the SPE, Paper 131350.
- Qin, X., D.-H. Han, and L. Zhao, 2014, Rock physics modeling of organic-rich shales with different maturity levels: 84th Annual International Meeting, SEG, Expanded Abstracts, 2952–2957.
- Ruiz, F. J., 2009, Porous grain model and equivalent elastic medium approach for predicting effective elastic properties of sedimentary rocks: Ph.D. dissertation, Stanford University.
- Sayers, C. M., 2013, The effect of anisotropy on the Young's moduli and Poisson's ratios of shales: *Geophysical Prospecting*, **61**, 416–426, doi: [10.1111/gpr.2013.61.issue-2](https://doi.org/10.1111/gpr.2013.61.issue-2).
- Sone, H., 2012, Mechanical properties of shale gas reservoir rocks and its relation to the in-situ stress variation observed in shale gas reservoirs: Ph. D. thesis, Stanford University.
- Sone, H., and M. D. Zoback, 2013, Mechanical properties of shale gas reservoir rocks — Part 1: Static and dynamic elastic properties and anisotropy: *Geophysics*, **78**, no. 5, D381–D392, doi: [10.1190/geo2013-0050.1](https://doi.org/10.1190/geo2013-0050.1).
- Tissot, B., B. Durand, J. Espitalie, and A. Combaz, 1974, Influence of nature and diagenesis of organic matter in formation of petroleum: *AAPG Bulletin*, **58**, 499–506.
- Vanorio, T., T. Mukerji, and G. Mavko, 2008, Emerging methodologies to characterize the rock physics properties of organic-rich shales: *The Leading Edge*, **27**, 780–787, doi: [10.1190/1.2944163](https://doi.org/10.1190/1.2944163).
- Vasin, R., H.-R. Wenk, W. Kanipanyacharoen, S. Matthies, and R. Wirth, 2013, Elastic anisotropy modeling of Kimmeridge shale: *Journal of Geophysical Research: Solid Earth*, **118**, 3931–3956, doi: [10.1002/jgrb.50259](https://doi.org/10.1002/jgrb.50259).
- Vernik, L., 1993, Microcrack-induced versus intrinsic elastic anisotropy in mature HC-source shales: *Geophysics*, **58**, 1703–1706, doi: [10.1190/1.1443385](https://doi.org/10.1190/1.1443385).
- Vernik, L., and A. Nur, 1992, Ultrasonic velocity and anisotropy of hydrocarbon source rocks: *Geophysics*, **57**, 727–735, doi: [10.1190/1.1443286](https://doi.org/10.1190/1.1443286).
- Vernik, L., and C. Landis, 1996, Elastic anisotropy of source rocks: Implications for hydrocarbon generation and primary migration: *AAPG Bulletin*, **80**, 531–544.
- Vernik, L., and J. Milovac, 2011, Rock physics of organic shales: *The Leading Edge*, **30**, 318–323, doi: [10.1190/1.3567263](https://doi.org/10.1190/1.3567263).
- Vernik, L., and X. Liu, 1997, Velocity anisotropy in shales: A petrophysical study: *Geophysics*, **62**, 521–532, doi: [10.1190/1.1444162](https://doi.org/10.1190/1.1444162).
- Walls, J. D., and E. Diaz, 2011, Relationship of shale porosity permeability trends to pore type and organic content: Denver Well Logging Society, *Petrophysics in Tight Oil Workshop*.
- Walls, J. D., and S. W. Sinclair, 2011, Eagle Ford shale reservoir properties from digital rock physics: *First Break*, **29**, 97–101.
- Xu, S., 1998, Modelling the effect of fluid communication on velocities in anisotropic porous rocks: *International Journal of Solids and Structures*, **35**, 4685–4707, doi: [10.1016/S0020-7683\(98\)00090-0](https://doi.org/10.1016/S0020-7683(98)00090-0).
- Xu, S., and R. E. White, 1995, A new velocity model for clay-sand mixtures: *Geophysical Prospecting*, **43**, 91–118, doi: [10.1111/gpr.1995.43.issue-1](https://doi.org/10.1111/gpr.1995.43.issue-1).
- Yan, F., and D. Han, 2013, Measurement of elastic properties of kerogen: 83rd Annual International Meeting, SEG, Expanded Abstracts, 2778–2782.
- Yenugu, M., 2014, Elastic, microstructural and geochemical characterization of kerogen maturity for shales: Ph.D. dissertation, University of Houston.
- Yenugu, M., and D.-H. Han, 2013, Seismic characterization of kerogen maturity: An example from Bakken shale: 83rd Annual International Meeting, SEG, Expanded Abstracts, 2773–2777.
- Zargari, S., M. Prasad, K. C. Mba, and E. D. Mattson, 2013, Organic maturity, elastic properties and textural characteristics of self-resourcing reservoirs: *Geophysics*, **78**, no. 4, D223–D235, doi: [10.1190/geo2012-0431.1](https://doi.org/10.1190/geo2012-0431.1).
- Zeszotarski, J. C., R. R. Chromik, R. P. Vinci, M. C. Messmer, R. Michels, and J. W. Larsen, 2004, Imaging and mechanical property measurements of kerogen via nano indentation: *Geochimica et Cosmochimica Acta*, **68**, 4113–4119, doi: [10.1016/j.gca.2003.11.031](https://doi.org/10.1016/j.gca.2003.11.031).
- Zhao, L., D. Han, Q. Yao, R. Zhou, and F. Yan, 2015, Seismic reflection dispersion due to wave-induced fluid flow in heterogeneous reservoir rocks: *Geophysics*, **80**, no. 3, D221–D235, doi: [10.1190/geo2014-0307.1](https://doi.org/10.1190/geo2014-0307.1).
- Zhao, L., M. Nasser, and D. Han, 2013, Quantitative geophysical pore type characterization and geological implications in carbonate reservoir: *Geophysical Prospecting*, **61**, 827–841, doi: [10.1111/gpr.2013.61.issue-4](https://doi.org/10.1111/gpr.2013.61.issue-4).
- Zhu, Y., S. Xu, M. Payne, A. Martinez, E. Liu, C. Harris, and K. Bandyopadhyay, 2012, Improved rock physics model for shale gas reservoirs: 82nd Annual International Meeting, SEG, Expanded Abstracts, doi: [10.1190/segam2012-0927.1](https://doi.org/10.1190/segam2012-0927.1).